A five equation model for the simulation of the two-phase flow in cryogenic coaxial injector

Angelo Murrone, Aymeric Boucher, Pierre Cordesse

SP2018_paper 222

A FIVE EQUATION MODEL FOR THE SIMULATION OF THE TWO-PHASE FLOW IN CRYOGENIC COAXIAL INJECTOR

Angelo MURRONE[(1)], Aymeric BOUCHER[(2)], Pierre CORDESSE[(3)]
[(1) (2) (3)]*ONERA - The French Aerospace Lab, F-92322 Châtillon, France*
[(1)]*angelo.murrone@onera.fr,* [(2)]*aymeric.boucher@onera.fr,* [(3)]*pierre.cordesse@onera.fr*

KEYWORDS: liquid rocket engines, numerical simulation, diffuse interface modelling, coupling, primary atomization

ABSTRACT:
In this paper, we propose models and methods for the simulation of two-phase flows in Liquid Rocket Engines (LRE) under subcritical conditions. The numerical strategy consists into coupling models dedicated to different topologies. Actually, we propose a five equation diffuse interface model for the treatment of the dense "separated two-phase flow" near the injector and an Eulerian kinetic based model for the "dispersed two-phase flow" in the chamber. We derive a novel formulation of the 5 equation system to build a robust HLLC type scheme. Then we use a fully Eulerian coupling strategy to take into account for primary atomization. We first run classical test cases in order to validate the numerical methods. Then a simulation on a test case representative to one coaxial injector is performed under subcritical conditions.

1. INTRODUCTION

To help the development and enhancement of launcher propulsion systems and to ensure their reliability, great care must be taken to study all the physical processes involved in the combustion chamber. Concerning liquid propulsion, this is a major issue which concerns a large variety of multi-scale phenomena such as evaporation, combustion, turbulence, primary atomization and break-up droplets. Moreover high frequency (HF) instabilities resulting from the complex interaction between propellants injection, flame dynamics and acoustic modes have been encountered in the recent past and have to be studied in a more comprehensive way. In this study, we focus on injection and primary atomization which play a key role to control the combustion under transient operating conditions and have also an influence on HF instabilities. As a result, one of the long term objectives for the launcher industry is to better understand under which conditions the atomization process tends to generate or amplify these HF instabilities, and under which conditions it has the opposite effect. We expect that CFD tools combined with experiments will eventually help to achieve this goal.

Figure 1 represents the different phenomena occurring at the exit of one coaxial cryogenic injector within a liquid rocket engine (LRE) operating in the subcritical regime. Under such conditions, the oxidizer (oxygen) exits the injector in liquid form whereas the fuel (hydrogen) is in gaseous form, which consequently entails a two-phase flow. Initial breakup of the bulk liquid, which is called primary atomization, occurs near the injector exit due to the strong difference of velocity between the two phases. The subsequent disintegration into child droplets due to secondary fragmentation occurs downstream. Following the classification of Ishii [20] this two-phase flow covers the entire range of volume fraction. In the dense region of the liquid jet, the atomization results from interaction between liquid oxygen (LOx) and gaseous hydrogen (GH_2) phases. Ligaments start growing from the liquid core because of Kelvin-Helmholtz and Rayleigh-Taylor interfacial instabilities [33]. The ligaments thus formed are unstable because disruptive forces exceed the liquid surface tension and viscous forces. This results in a spray of small LOx droplets with final stable sizes, mainly spherical, which are dispersed by the turbulent gas flow and finally vaporized to feed the combustion with GH_2. Thus the gas phase is a mixture of multiple chemical species, namely hydrogen, vaporized oxygen and combustion products. Eventually, the resulting high-enthalpy combustion products exhaust through a nozzle at supersonic speed, thereby providing the required thrust.

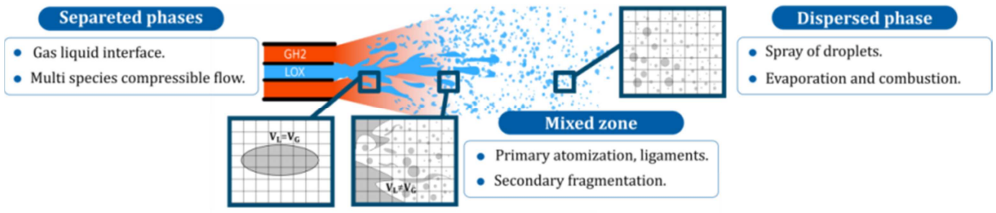

Figure 1: schematic representation of a coaxial cryogenic injector

A lot of experimental and theoretical studies were conducted on the atomization process but the details of the breakup cascade are still not fully understood. There are no sufficient results to provide parameters like the expansion angle, the penetration depth or the droplet size distribution. Regarding experimentation, the main reason lies in the droplets cloud surrounding the liquid core region which block the access to optical rays. Moreover, it is difficult to view phenomena because the length and time characteristics are very small. Nevertheless, with recent improvements in optical ray and x-ray imaging techniques, a detailed analysis of gas liquid interface has been provided in [33]. For the MASCOTTE cryogenic injector [44], the spray was recently investigated with a high speed camera in a backlighting optical configuration [29]. On the other hand, experiments concerning diesel injection are gaining importance [45], [9], [35]. We expect that in a near future, spatial resolution at the sub-micrometer level may provide databases for cryogenic rocket engines but also for Direct Diesel Injection.

Concerning numerical simulation, computational resources give us the possibility to view the atomization process more accurately than before and DNS are gaining importance [15], [12], [18], [19]. A lot of works are thus based on the ARCHER software [32] which combines both Level Set and VOF methods. In [14], the DNS of a two-phase flow provides very promising results. Nevertheless, the finest scales of two-phase flows are not known a priori, contrary to the Kolmogorov scale, and moreover cannot be resolved even if the mesh size is below the micrometer scale. Other recent works of DNS can also be mentioned [4] but it seems that DNS is not mature enough for industrial configurations.

Leaving DNS aside, we can find in the literature various numerical works based on the RANS or LES formalisms where the primary atomization is not taken into account. In this kind of approach, the parameters giving the initial properties of the spray such as droplets size and velocity distribution are given as presumed input data in the numerical simulation. Consequently we cannot rely on these models to simulate complex unsteady phenomena in which primary atomization plays a key role (as it is for instance highly suspected with HF instabilities in LRE). We need to derive numerical models, within the RANS or LES frameworks, valid from the primary atomization of the liquid jet, to the computation of the spray without having to impose its properties as input parameters.

This quest has been initiated in the seminal work of [40], [42], [43] and was pursued by many subsequent works, most of them applied to Direct Diesel Injection in internal combustion engines but also sometimes to cryogenic rocket engines [36], [21], [22], [27], [10]. All these works involve a sophisticated surface density equation (see [28] for theoretical analysis of such an equation) that contains source terms for creation and destruction of interface area. These source terms are closed within the RANS framework of turbulence, thanks to sub-grid models derived from theoretical, experimental or DNS results [14]. A similar surface density equation is used in an LES context in [6], [7], [8] together with accurate tracking interface methods. Another interesting work in this context is the recent one presented in [11] which deals with the liquid jet atomization under Direct Diesel engine conditions, but without considering combustion. In the latter, the authors retain a 7 equation diffuse interface model [5] together with relaxation procedures for pressure, velocity [38] and temperature [46], which they use for both the liquid core and the spray droplets. A new atomization model is also formulated using two surface density equations and the closure terms are based on RANS simulations, the description of the turbulence being necessary for both liquid and gas phases. Using two surface density equations is a novelty since all previous works necessitated a unique surface density equation. The two surface density equations are transported with the same interface velocity; one for the dense “separated” phases and another one for the “dispersed” phase.

The objective is to improve both the primary atomization and the secondary breakup modelling. Besides, in [1], a quasi-multiphase Eulerian (QME) solver is implemented in OpenFOAM and applied to a jet in crossflow. Comparisons with experiments and DNS of [18], [19] are presented. The innovative second order closure for the slip velocity is based on transport equations for momentum, volume fraction, surface density and liquid flux. It is therefore an intermediate approach between fully multiphase and mixture approaches since it holds for a large range of liquid volume fraction going from dense "separated" to dilute "dispersed" flow.

Based on the above-mentioned works, the idea of coupling the "RANS equations plus surface density equation" strategy with a Lagrangian description for the spray was introduced by work presented in [2], which has led to the development of the dedicated ELSA (Eulerian Lagrangian Spray Atomization) code. The idea is to reach a better overall accuracy by allowing the spray to be described with its own variables (velocity, size, temperature), rather than describing it only through the surface density equation and the mean velocity and temperature of the whole sub-grid liquid-gas mixture. Following this strategy, the subsequent works of [25], [26] made the source terms depend on whether the topology of the two-phase flow is "dispersed" or "separated", and they also improved the definition of the equilibrium Weber number. However it seems that the strong coupling between Eulerian and Lagrangian methods induces some difficulties [13]. In [18], an efficient parallel multi-scale coupling procedure between an Eulerian level set method tracking interface and a Lagrangian description of small scales has been applied successfully to a turbulent liquid jet under Diesel engine conditions, but again with some remaining numerical difficulties. Indeed, several difficulties may arise when dealing with Eulerian - Lagrangian methods. The first one is due to the lack of robustness of the Lagrangian methods in the case of a strong two-way coupling. The second one is due to the statistical interpretation of numerous numerical particles produced in the atomization area. It seems also that taking into account for the compressibility of the fluid with the tracking interface method is not an easy task. In the Eulerian-Eulerian methods, the major drawbacks are that numerics are possibly tricky when solving the spray equations (discontinuities, weak hyperbolicity...), and also that the description of the phenomena at the droplet scale may be more complex than in the Lagrangian formalism. But one major advantage against interface tracking and Lagrangian methods is that models are general, fully compressible and adapted to the two-way coupling simulations. Moreover, Eulerian-Eulerian methods are also well adapted to parallel and time implicit computations.

This is why we follow in this paper a fully Eulerian coupling strategy between "separated" and "dispersed" two-phase flow models for the simulation of primary atomization, introduced in [29], [31], [16]. It combines a kinetic-based model for the description of the spray with a diffuse interface model to describe both the "separated" and "mixed" two-phase flows. This work has been conducted in the framework of the multi-physics CEDRE platform [37], [34] developed at ONERA and applied to the cryogenic MASCOTTE facility [44] representative of one coaxial injector of a liquid rocket engine.

In a previous works [31], we have proposed a coupling strategy between a 4 equation diffuse interface model and an Eulerian kinetic model for the spray. The fully Eulerian coupling between "separated" and "dispersed" two-phase flow solvers has been applied to the simulation of the MASCOTTE [17], [44], [41], [29] test facility on the 10-bar operating point corresponding to cryogenic rocket engines under transient operating conditions as depicted in Figure 2.

In this paper, we focus on the improvement of the diffuse interface model for the simulation of separated two-phase flow in coaxial cryogenic injector in order to realize the same coupling strategy. Instead of using the 4 equation model, we have selected the 5 (two temperatures) equation model which can be obtained by velocity and pressure relaxation of the 7 equation model [5]. The two temperatures of the 5 equation model [30] provide an accurate description of the liquid temperature and is able to avoid spurious pressure oscillations of the 4 equation model due to mixing of hot gas with cold liquid in the diffuse interface.

The derivation of the 5 equation model is presented in the next section 2. Moreover, we give some details on the HLLC schemes [3] we have implemented in the code. We also present briefly the coupling strategy together and the atomization model we have used. Finally in section 3, we present the numerical results obtained on validation test cases and on a coaxial injector configuration in subcritical conditions. A brief conclusion is addressed at the end of the paper. Finally, we draw the principal perspectives.

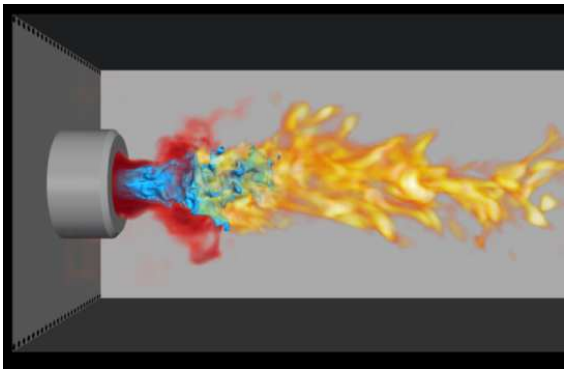

Figure 2: LES of a subcritical combustion LOx/GH2 (10-bar operating MASCOTTE 10 facility) (Liquid oxygen in blue, hydrogen in red and flame in yellow)

2. MODELS AND METHODS

For the simulation of liquid gas interface, we point out that diffuse interface modelling are gaining importance [39], [24]. The coupling is necessary because we want to deal with transition from dense to dilute concentration of the liquid phase and interface and kinetic models present fundamental differences. More specifically, in the dilute limit, diffuse interface models involve acoustic waves propagation which are not correct. Moreover, in kinetic models, the volume occupied by liquid is neglected and particles are considered as incompressible. In the framework of diffuse interface modelling, different levels of description are available. Modelling of two-phase flows is typically based on averaging procedures [20]. In their most general form, these averaging techniques produce models characterized by two different velocities and pressures for each phase supplemented by one or several topological equations. This is namely the 7 equation model [5], [38]. As usual, a delicate balance between the complexity of the model and its performance has to be found. In the dense region of the two-phase flow, we propose to use a 5 equation model providing two different temperatures, one for the liquid and another one for the gas.

2.1 The 7 equation model

If we extend this 7 equation model to the case of multi-species fluid, mass conservation equation may be readily replaced by mass fractions equations and the convective part of the (5+n_1+n_2) equations system with relaxation pressures, velocities and temperatures source terms can be written under the form below. Moreover, the two terms $Q = \theta(T_2 - T_1), m = \nu(g_2 - g_1)$ in the system stand respectively for the heat and mass transfer.

$$\frac{\partial(\alpha_1\rho_1 Y_1^i)}{\partial t} + div(\alpha_1\rho_1 Y_1^i \boldsymbol{u}_1) = w_1^i$$

$$\frac{\partial(\alpha_1\rho_1 \boldsymbol{u}_1)}{\partial t} + div(\alpha_1\rho_1 \boldsymbol{u}_1 \otimes \boldsymbol{u}_1) + \nabla(\alpha_1 p_1) = p_I \nabla\alpha_1 + \lambda(\boldsymbol{u}_2 - \boldsymbol{u}_1) + \boldsymbol{u}_I m$$

$$\frac{\partial(\alpha_1\rho_1 e_1)}{\partial t} + div(\alpha_1(\rho_1 e_1 + p_1)\boldsymbol{u}_1) = p_I \boldsymbol{u}_I \cdot \nabla\alpha_1 + \lambda \boldsymbol{u}_I \cdot (\boldsymbol{u}_2 - \boldsymbol{u}_1) + p_I\mu(p_2 - p_1) + Q + \left(e_I + \frac{\boldsymbol{u}_I^2}{2}\right)m$$

$$\frac{\partial(\alpha_2\rho_2 Y_2^i)}{\partial t} + div(\alpha_2\rho_2 Y_2^i \boldsymbol{u}_2) = w_2^i$$

$$\frac{\partial(\alpha_2\rho_2 \boldsymbol{u}_2)}{\partial t} + div(\alpha_2\rho_2 \boldsymbol{u}_2 \otimes \boldsymbol{u}_2) + \nabla(\alpha_2 p_2) = -p_I \nabla\alpha_1 - \lambda(\boldsymbol{u}_2 - \boldsymbol{u}_1) - \boldsymbol{u}_I m$$

$$\frac{\partial(\alpha_2\rho_2 e_2)}{\partial t} + div(\alpha_2(\rho_2 e_2 + p_2)\boldsymbol{u}_2) = -p_I \boldsymbol{u}_I \cdot \nabla\alpha_1 - \lambda \boldsymbol{u}_I \cdot (\boldsymbol{u}_2 - \boldsymbol{u}_1) - p_I\mu(p_2 - p_1) - Q - \left(e_I + \frac{\boldsymbol{u}_I^2}{2}\right)m$$

$$\frac{\partial\alpha_1}{\partial t} + \boldsymbol{u}_I \cdot \nabla\alpha_1 = \mu(p_1 - p_2) + \frac{Q}{\kappa} + \frac{m}{\varrho} \quad \text{Eq. 1}$$

The notations are classical. Firstly, α_k are the volume fractions of each phase ($\alpha_1 + \alpha_2 = 1$), ρ_k the phase densities, $\boldsymbol{u}_k$ the vector velocities, p_k the pressures and $e_k = \varepsilon_k + \boldsymbol{u}_k^2/2$ the specific total energies, with ε_k the specific internal energies. On the other hand, $\boldsymbol{u}_I, p_I$ stand for the interfacial velocity and pressure for which we have chosen the following expressions:

$$\boldsymbol{u}_I = \frac{\sum_{k=1}^2 \alpha_k\rho_k\boldsymbol{u}_k}{\sum_{k=1}^2 \alpha_k\rho_k}, \qquad p_I = \sum_{k=1}^2 \alpha_k p_k \quad \text{Eq. 2}$$

2.2 The 5 equation model

The general 7 equation model contains relaxation parameters λ and μ which determine the rates at which velocities and pressures of the two phases reach equilibrium. Here we are interested in situations where relaxation times are small compared with the other physical characteristic times. From an asymptotic analysis, one can derive a five equation reduced model with a single velocity and pressure. The original formulation includes an equation for the volume fraction and one for the total mixture energy. This (3+n_1+n_2) equation system [30] extended here to the multi-species case will be referred to as the ''(e,α) formulation''. The system writes:

$$\frac{\partial(\alpha_1\rho_1Y_1^i)}{\partial t}+div(\alpha_1\rho_1Y_1^i\boldsymbol{u})=0$$

$$\frac{\partial(\alpha_2\rho_2Y_2^i)}{\partial t}+div(\alpha_2\rho_2Y_2^i\boldsymbol{u})=0$$

$$\frac{\partial(\rho\boldsymbol{u})}{\partial t}+div(\rho\boldsymbol{u}\otimes\boldsymbol{u})+\nabla p=0$$

$$\frac{\partial(\rho e)}{\partial t}+div((\rho e+p)\boldsymbol{u})=0$$

$$\frac{\partial\alpha_1}{\partial t}+\boldsymbol{u}\cdot\nabla\alpha_1=\alpha_1\alpha_2\frac{\rho_2a_2^2-\rho_1a_1^2}{\alpha_1\rho_2a_2^2+\alpha_2\rho_1a_1^2}div(\boldsymbol{u}) \quad \text{Eq. 3}$$

Now, we establish a formulation of this reduced model using two equations of transport for the internal energies instead of an equation for the volume fraction and another for the total mixture energy. If the different formulations are equivalent for smooth solutions, we expect the second one to be more adapted for non-conservative term. This second formulation of the 5 equation system will be referred to as the ''(ε_1,ε_2) formulation''. Thus we set $\lambda=\lambda_0/\varepsilon$ and $\mu=\mu_0/\varepsilon$ where ε tends to zero and we look for limit equations of the 7 equation model. In this way, we use an asymptotic expansion in terms of ε and we try to establish the governing equations when $\varepsilon\to 0$. This analysis can be performed directly on the conservative form of the system. However it is more convenient to work with the set of variables $(\alpha_k\rho_k,\boldsymbol{u}_k,\varepsilon_k,p_k,\alpha_k)$ and to use the quasi-linear form of the equations as in the following. Using the notation $D_k/Dt=\partial_t+\boldsymbol{u}_k\cdot\nabla$ for the material derivative, from the momentum and the mass conservation equations, it is easily seen that the velocities $\boldsymbol{u}_k$ obey:

$$\alpha_k\rho_k\frac{D_k\boldsymbol{u}_k}{Dt}+\nabla(\alpha_kp_k)=p_I\nabla\alpha_k+\lambda(\boldsymbol{u}_{k'}-\boldsymbol{u}_k) \quad \text{Eq. 4}$$

From these last equations, we deduce the ones for the kinetic energy $\boldsymbol{u}_k^2/2$ of each phase:

$$\alpha_k\rho_k\frac{D_k(\boldsymbol{u}_k)^2/2}{Dt}+\boldsymbol{u}_k\cdot\nabla(\alpha_kp_k)=p_I\boldsymbol{u}_k\cdot\nabla\alpha_k+\lambda\boldsymbol{u}_k\cdot(\boldsymbol{u}_{k'}-\boldsymbol{u}_k) \quad \text{Eq. 5}$$

Then from the total energy equations, we get the equations for the specific internal energies:

$$\alpha_k\rho_k\frac{D_k\varepsilon_k}{Dt}+\alpha_kp_kdiv(\boldsymbol{u}_k)=p_I(\boldsymbol{u_I}-\boldsymbol{u}_k)\cdot\nabla\alpha_k+\mu p_I(p_{k'}-p_k)+\lambda(\boldsymbol{u_I}-\boldsymbol{u}_k)\cdot(\boldsymbol{u}_{k'}-\boldsymbol{u}_k) \quad \text{Eq. 6}$$

Now, we suppose a binary law state $\varepsilon_k=\varepsilon_k(\rho_k,p_k)$ and introduce the coefficients χ_k,κ_k for the partial derivatives:

$$\chi_k=\frac{\partial\varepsilon_k}{\partial\rho_k}\Big|_{p_k},\ \kappa_k=\frac{\partial\varepsilon_k}{\partial p_k}\Big|_{\rho_k} \quad \text{Eq. 7}$$

After some calculations, the transport equations for the pressures write:

$$\alpha_k\frac{D_kp_k}{Dt}+\alpha_kC_kdiv(\boldsymbol{u}_k)=C_{kI}(\boldsymbol{u_I}-\boldsymbol{u}_k)\cdot\nabla\alpha_k+\mu C_{kI}(p_{k'}-p_k)+\frac{\lambda}{\kappa_k\rho_k}(\boldsymbol{u_I}-\boldsymbol{u}_k)\cdot(\boldsymbol{u}_{k'}-\boldsymbol{u}_k) \quad \text{Eq. 8}$$

In these last equations, we have introduced the phasic sound speeds $a_k$and the acoustic impedances C_k. Then, the notations a_{kI},C_{kI} stand for the same quantities evaluated at the interfaces:

$$a_k^2=\frac{\partial p_k}{\partial\rho_k}\Big|_{s_k}=\frac{1}{\kappa_k}\left(\frac{p_k}{\rho_k^2}-\chi_k\right),\quad a_{kI}^2=\frac{1}{\kappa_k}\left(\frac{p_I}{\rho_k^2}-\chi_k\right),\quad C_k=\rho_ka_k^2,\quad C_{kI}=\rho_ka_{kI}^2 \quad \text{Eq. 9}$$

Now, we perform the asymptotic analysis introducing the following expansion in term of ε for velocities and pressures but also for the other variables:

$$\boldsymbol{u}_k=\boldsymbol{u}^0+\varepsilon\boldsymbol{u}_k^1,\qquad p_k=p^0+\varepsilon p_k^1 \quad \text{Eq. 10}$$

The mass conservation equations at order 0 read:

$$\frac{\partial(\alpha_k^0\rho_k^0)}{\partial t}+div(\alpha_k^0\rho_k^0\boldsymbol{u}^0)=0 \quad \text{Eq. 11}$$

The equations for velocities at order 0 read:

$$\alpha_k^0\rho_k^0\left(\frac{\partial\boldsymbol{u}^0}{\partial t}+\boldsymbol{u}^0\cdot\nabla\boldsymbol{u}^0\right)+\nabla(\alpha_k^0p^0)=p^0\nabla\alpha_k^0+\lambda^0(\boldsymbol{u}_{k'}^1-\boldsymbol{u}_k^1) \quad \text{Eq. 12}$$

Then we can deduce at the order 0 the equations for internal energies and pressures:

$$\alpha_k^0\rho_k^0\left(\frac{\partial\varepsilon_k^0}{\partial t}+\boldsymbol{u}^0\cdot\nabla\varepsilon_k^0\right)+\alpha_k^0p^0div(\boldsymbol{u}^0)=\mu p^0(p_{k'}^1-p_k^1) \quad \text{Eq. 13}$$

$$\alpha_k^0\left(\frac{\partial p^0}{\partial t}+\boldsymbol{u}^0\cdot\nabla p^0\right)+\alpha_k^0C_k^0div(\boldsymbol{u}^0)=\mu^0C_k^0(p_{k'}^1-p_k^1) \quad \text{Eq. 14}$$

Then, combining the above equations, we can get the pressures fluctuations at the order 1:

$$\mu^0(p_2^1-p_1^1)=\alpha_1^0\alpha_2^0\frac{C_1^0-C_2^0}{\alpha_1^0C_2^0+\alpha_2^0C_1^0}\,div(\boldsymbol{u}^0) \quad \text{Eq. 15}$$

Now, if we use the equations at order 0 for internal energies, and we introduce the expression of the pressure fluctuations, we get:

$$\alpha_k^0\rho_k^0\left(\frac{\partial\varepsilon_k^0}{\partial t}+\boldsymbol{u}^0\cdot\nabla\varepsilon_k^0\right)+\alpha_k^0p^0div(\boldsymbol{u}^0)$$
$$=\alpha_k^0\alpha_{k'}^0p^0\frac{C_k^0-C_{k'}^0}{\alpha_k^0C_{k'}^0+\alpha_{k'}^0C_k^0}\,div(\boldsymbol{u}^0)\quad\text{Eq. 16}$$

Now using the mass conservation, internal energy equations read:

$$\frac{\partial(\alpha_k^0\rho_k^0\varepsilon_k^0)}{\partial t}+div(\alpha_k^0\rho_k^0\varepsilon_k^0\boldsymbol{u}^0)$$
$$=p^0\left(\frac{-\alpha_k^0C_{k'}^0}{\alpha_k^0C_{k'}^0+\alpha_{k'}^0C_k^0}\right)div(\boldsymbol{u}^0)\quad\text{Eq. 17}$$

Finally, the 5 equation model referred to as the ''(ε_1,ε_2) formulation'' can be written under the form below. This new formulation will be used for the design of numerical fluxes.

$$\frac{\partial(\alpha_1\rho_1Y_1^i)}{\partial t}+div(\alpha_1\rho_1Y_1^i\boldsymbol{u})=0$$
$$\frac{\partial(\alpha_2\rho_2Y_2^i)}{\partial t}+div(\alpha_2\rho_2Y_2^i\boldsymbol{u})=0$$
$$\frac{\partial(\rho\boldsymbol{u})}{\partial t}+div(\rho\boldsymbol{u}\otimes\boldsymbol{u})+\nabla p=0$$
$$\frac{\partial(\alpha_1\rho_1\varepsilon_1)}{\partial t}+div(\alpha_1\rho_1\varepsilon_1\boldsymbol{u})=p\left(\frac{-\alpha_1\rho_2a_2^2}{\alpha_1\rho_2a_2^2+\alpha_2\rho_1a_1^2}\right)div(\boldsymbol{u})$$
$$\frac{\partial(\alpha_2\rho_2\varepsilon_2)}{\partial t}+div(\alpha_2\rho_2\varepsilon_2\boldsymbol{u})$$
$$=p\left(\frac{-\alpha_2\rho_1a_1^2}{\alpha_1\rho_2a_2^2+\alpha_2\rho_1a_1^2}\right)div(\boldsymbol{u})\quad\text{Eq. 18}$$

2.3 HLLC schemes for the 5 equation model

In this section, we propose to resolve the model in a Finite Volume framework. A lot of works have been recently dedicated to liquid-gas interface problems. These types of two-phase flows exhibit strong gradients of variables and large variation of sound speed near the interface between the phases. In this context, it is mandatory to derive accurate but also very robust schemes. The class of HLLC schemes based on the approximated resolution of the non-linear Riemann problem seems to be a good candidate. For the 5 equation model, we have presented two formulations of the system. The first one is the ''(e,α) formulation'' and the one second is the ''(ε_1,ε_2) formulation''. The last one is very interesting and gives us the possibility to examine the most adapted closure of non-conservative terms satisfying total energy conservation. These shock computational difficulties due to non-conservative character of the model has to be examined carefully. This could help us to maintain positivity for crucial variables such as density, pressure or volume fraction. Then an extension of the multi-slope technique for this two-phase flow model and their specific variables has been implemented. When we are interested in two-phase flows, we have to deal with high density ratios, strong gradients and also discontinuous solutions. Nowadays, the MUSCL technique remains a good compromise between accuracy and robustness. For this reason, we have chosen the multi-slope approach for general unstructured meshes to cope with strong discontinuities of the flow.

$$V\frac{\partial Q}{\partial t}=\sum_{i=1}^{nfaces}(-\boldsymbol{F}_i\cdot S_i)-\iiint\boldsymbol{K}div(\boldsymbol{u})dV\quad\text{Eq. 19}$$

The conservative part of the flux read respectively for the ''(e,α)'' and the ''(ε_1,ε_2) formulations'':

$$\boldsymbol{F}_i\cdot S_i=\begin{bmatrix}\alpha_1\rho_1Y_1^iu_n\\ \alpha_2\rho_2Y_2^iu_n\\ \rho\boldsymbol{u}u_n+p\boldsymbol{n}\\ (\rho e+p)u_n\\ \alpha_1u_n\end{bmatrix},\quad\boldsymbol{F}_i\cdot S_i=\begin{bmatrix}\alpha_1\rho_1Y_1^iu_n\\ \alpha_2\rho_2Y_2^iu_n\\ \rho\boldsymbol{u}u_n+p\boldsymbol{n}\\ \alpha_1\rho_1\varepsilon_1u_n\\ \alpha_2\rho_2\varepsilon_2u_n\end{bmatrix}\quad\text{Eq. 20}$$

On the other hand, the non-conservative terms are given by the following expressions:

$$\boldsymbol{K}=\begin{bmatrix}0\\0\\0\\0\\-\frac{\alpha_1C_2}{\alpha_2C_1+\alpha_1C_2}\end{bmatrix},\qquad\boldsymbol{K}=\begin{bmatrix}0\\0\\0\\\alpha_1C_2\\p\frac{\alpha_1C_2}{\alpha_2C_1+\alpha_1C_2}\\p\frac{\alpha_2C_1}{\alpha_2C_1+\alpha_1C_2}\end{bmatrix}\quad\text{Eq. 21}$$

If we consider the vector $\boldsymbol{K}$ constant in the cell, we can proceed to integration;

$$V\frac{\partial Q}{\partial t}=\sum_{i=1}^{nfaces}-(\boldsymbol{F}_i+\boldsymbol{K}u_{n,i})\cdot S_i\quad\text{Eq. 22}$$

Then the conservative part of the flux at the interface is evaluated following the HLLC scheme described below. The wave velocities S_L, S_R, S_M are computed in a classical way and the intermediate states Q_L^*, Q_R^* in the star region read:

$$\frac{u_{n,L}-S_L}{S_M-S_L}\begin{pmatrix}\alpha_{k,L}\rho_{k,L}Y_{k,L}^i\\ \rho_L[\boldsymbol{u}_L+(S_M-u_{n,L})\boldsymbol{n}]\\ \rho_L\left[e_L+\frac{p_L}{\rho_L}\frac{u_{n,L}-S_M}{u_{n,L}-S_L}+(S_M-u_{n,L})S_M\right]\end{pmatrix},$$

$$\frac{u_{n,R}-S_R}{S_M-S_R}\begin{pmatrix}\alpha_{k,R}\rho_{k,R}Y_{k,R}^i\\ \rho_R[\boldsymbol{u}_R+(S_M-u_{n,R})\boldsymbol{n}]\\ \rho_R\left[e_R+\frac{p_R}{\rho_R}\frac{u_{n,R}-S_M}{u_{n,R}-S_R}+(S_M-u_{n,R})S_M\right]\end{pmatrix}\text{Eq. 23}$$

Then the HLLC flux can be written under the form:

$$F = \frac{F_L + F_R}{2} + \frac{\sigma_L + \sigma_R}{2}\frac{F_L - F_R}{2} + \frac{\sigma_R - \sigma_L}{2}\left[\frac{S_L}{2}(Q_L^* - Q_L) + \frac{S_R}{2}(Q_R^* - Q_R) + \sigma_M \frac{S_M}{2}(Q_L^* - Q_R^*)\right]$$

$$\sigma_L = sign(S_L), \sigma_R = sign(S_R), \sigma_M = sign(S_M) \quad \text{Eq. 24}$$

First, we consider the ''(e,α) formulation'' of the model and the only one non conservative equation for the volume fraction writes:

$$V\frac{\partial \alpha_1}{\partial t} = \sum_{i=1}^{nfaces} -\left[(\widehat{\alpha_1 u_n})_i + \boldsymbol{K}\hat{u}_{n,i}\right]S_i \quad \text{Eq. 25}$$

Then, according to the sign of the waves S_L , S_R, S_M , we are able to compute:

$$(\widehat{\alpha_1 u_n})_i = \left(\alpha_{1,L}u_{n,L}, \alpha_{1,L}^* S_M, \alpha_{1,R}^* S_M, \alpha_{1,R}u_R\right),$$
$$\hat{u}_{n,i} = \left(u_{n,L}, S_M, S_M, u_R\right) \quad \text{Eq. 26}$$

Then combining, the two components of the mass fractions (Eq. 23) in the star region, the volume fractions read:

$$\alpha_{1,L}^* = \frac{R_L}{1+R_L}, \qquad R_L = \frac{(\alpha_1\rho_1)_L}{(\alpha_2\rho_2)_L}\frac{\rho_{2,L}^*}{\rho_{1,L}^*},$$

$$\alpha_{1,R}^* = \frac{R_R}{1+R_R}, \qquad R_L = \frac{(\alpha_1\rho_1)_R}{(\alpha_2\rho_2)_R}\frac{\rho_{2,R}^*}{\rho_{1,R}^*} \quad \text{Eq. 27}$$

Then, let us suppose isentropic rarefaction across the waves S_L , S_R and we can deduce the real phasic density:

$$\rho_{k,L}^* - \rho_{k,L} = \frac{p_L^* - p_L}{\hat{a}_{k,L}^2}, \quad \rho_{k,R}^* - \rho_{k,R} = \frac{p_R^* - p_R}{\hat{a}_{k,R}^2} \quad \text{Eq. 28}$$

Now, we consider the second ''(ε_1,ε_2) formulation'' of the 5 equation model. We have to deal with the non-conservative equations for the internal energy of each phase:

$$V\frac{\partial \alpha_k\rho_k\varepsilon_k}{\partial t} = \sum_{i=1}^{nfaces}\left[-(\widehat{\alpha_k\rho_k\varepsilon_k u_n})_i + \boldsymbol{K}\hat{u}_{n,i}\right]S_i \quad \text{Eq. 29}$$

Then, according to the sign of the waves S_L , S_R, S_M , we are able to compute:

$$(\widehat{\alpha_k\rho_k\varepsilon_k u_n})_i = \left((\alpha_k\rho_k)_L\varepsilon_{k,L}u_L, (\alpha_k\rho_k)_L^*\varepsilon_{k,L}^* S_M, (\alpha_k\rho_k)_R^*\varepsilon_{k,R}^* S_M, (\alpha_k\rho_k)_R\varepsilon_{k,R}u_R\right),$$
$$\hat{u}_{n,i} = \left(u_{n,L}, S_M, S_M, u_R\right) \quad \text{Eq. 30}$$

Now we have to determine the values of internal energies in the star region $\varepsilon_{k,L}^*, \varepsilon_{k,R}^*$ which are the only unknowns. We have implemented and tested different solutions presented below.

$$\varepsilon_{k,L}^* = \varepsilon_{k,L} \quad option\ (a)$$
$$\varepsilon_{k,L}^* = \varepsilon\left(\rho_{k,L}^*, p^*\right) \quad option\ (b)$$
$$T_{k,L}^* = T_{k,L}, \varepsilon_{k,L}^* = \varepsilon\left(T_{k,L}^*, p^*\right) \quad option\ (c)$$
$$\varepsilon_k^* - \varepsilon_k = (p + p^*)(v - v^*)/2 \quad option\ (d)$$

$$(\alpha_k\rho_k\varepsilon_k)^{corrected} = \alpha_k\rho_k\varepsilon_k + K_k\Delta(\rho\varepsilon),$$
$$K_1 + K_2 = 1 \ option\ (e) \quad \text{Eq. 31}$$

2.4 Coupling strategy and atomization model

The classical source terms between the diffuse interface model and the kinetic model are the drag force (velocity relaxation), the heat transfer (temperature relaxation) and the mass transfer.

$$F_D, \phi_C, \dot{m}_{vap} \quad \text{Eq. 32}$$

The correlation of Schiller-Naumann is used for the drag force and the Abramzon-Sirignano model is used for the heat and mass transfer. Now we describe the source terms s(u) for the spray solver and then focus on the primary atomization. The first component traduces the growth of mass due to primary atomization and its decrease by vaporization. If we now look at the source term S(U) affected to the carrier phase. The first ng components of gas species concern combustion and evaporation phenomena. The first term includes the evaporation of liquid oxygen droplets in the "dispersed" phase which creates gas oxygen in the carrier phase. The component number ng +1 standing for the transport equation of mass liquid fraction concerns primary atomization. It transforms the dense LOx into "dispersed" LOx.

$$s(u) = \begin{bmatrix} s_{\rho_d} \\ s_{\rho_d v_d} \\ s_{\rho_d h_d} \\ s_{N_d} \end{bmatrix} = \begin{bmatrix} \dot{m}_{ato} - N_d\dot{m}_{vap} \\ s_{\rho_d}v_d + N_d F_D \\ s_{\rho_d}h_d + N_d(F_D \cdot v_d + \phi_C) \\ \dot{N}_{ato} \end{bmatrix}$$

$$S(U) = \begin{bmatrix} s_{\rho Y_{O2}} \\ s_{\rho Y_l} \\ \vdots \\ s_{\rho Y_{ng}} \\ s_{\rho Y_l} \\ S_v \\ S_e \end{bmatrix} = \begin{bmatrix} \dot{w}_{O2} + N_d\dot{m}_{vap} \\ \dot{w}_l \\ \vdots \\ \dot{w}_{ng} \\ -\dot{m}_{ato} \\ -s_{\rho_d v_d} \\ -s_{\rho_d h_d} \end{bmatrix} \quad \text{Eq. 33}$$

The model used to describe the mass transfer between solvers accounting for primary atomization reads in:

$$\dot{m}_{ato} = \rho Y_l \nu_{ato}\lambda_{ato}(Y_l) \quad \text{Eq. 34}$$

where ρY_l is the liquid mass in a given volume of control, ν_{ato} is the characteristic frequency of the primary atomization process, and $\lambda_{ato}(Y_l)$ is an efficiency function. We assume the atomization frequency to be directly connected to the strength of the velocity gradient, which is the only information locally available in the 5 equation model. This could be estimated using several approaches, amongst which the Q criterion, the vorticity or the resolved strain tensor, all being based on the velocity gradient. In this study we have chosen to use the latter approach:

$$\nu_{turb} = \sqrt{2D^2}\, D^2 = \sum_{ij} D_{ij} D_{ij} \qquad D_{ij} = \frac{1}{2}\left(\frac{\partial \bar{u}_i}{\partial x_j} + \frac{\partial \bar{u}_j}{\partial x_i}\right) \text{ Eq. 35}$$

The efficiency function reads in [29]. It is designed to make sure that when some LOx mass is transferred from the fluid towards the spray in a given volume of control the corresponding vanishing volume in the fluid is actually negligible. Otherwise the gas would experience some unphysical expansion in the volume control, which obviously has to be avoided, and the dispersed hypothesis made for the spray would not be respected. In other words, we use the numerical diffusion which spreads the interface over several mesh elements in order to carry out the mass transfer in a smooth way. As this point with this 5 equation model, except for the temperature, the properties of the created droplets resulting from the primary atomization have to be presumed. Actually, these properties are estimated based on the instability analysis from Villermaux [33]. In the latter work, the drop size and velocity distributions of the spray are estimated as a function of the injected propellant properties (density ratio, inlet velocities, vorticity thickness...). Consequently, the knowledge of the steady operating conditions of the MASCOTTE configuration under study permits to derive an overall mean droplet diameter subsequent to the primary atomization process and a corresponding mean droplet velocity. The direction given to the droplet velocity in each mesh cell has been set to that of the fluid, which may be actually a rough approximation. Finally, the temperature of the created droplet is the LOx dense temperature of the interface diffuse model. This is the first advantage of the 5 equation model. The second one is the correct description of the thermodynamic mixture between liquid and gas. Therefore the spurious pressure and temperature oscillations encountered in the 4 equation model at the interfaces are now prevented.

3. RESULTS

3.1 Water-air shock tube

The length of the domain is 1 m and initially the interface is located at x = 0.7 m. The tube is initially filled with high pressure liquid water on the left side and with air on the right side. This test problem consists of a classical shock tube with two fluids and admits an exact solution. The initial condition consists in a pressure discontinuity between p = 10^9 Pa in the liquid side and p = 10^5 Pa in the gas side. The right and left chambers contain nearly pure fluids: the volume fraction of the gas in the water chamber is 10^{-8} and inversely the water volume fraction is 10^{-8} in the gas chamber. Figure 3 displays for the different numerical methods the volume fraction, the mixture density, the pressure and the velocity. The exact solutions are represented on these curves. The results are shown at time 229µs and seem to be of comparable accuracy with respect to the exact solution. Figure 3 plots the results at the order 1 in space. For the monophasic variables such as the temperatures, we emphasize that different schemes could give very different results and don't have the same robustness. Nevertheless, the formulation with two internal energies seems very promising compared to the one with the volume fraction and total energy transport equations. For the simulations, a Stiffened Gas equation of state [23] has been implemented for each phase. It takes into account for attractive and repulsive molecular effects.

$$p_k = (\gamma_k - 1)\rho_k(\varepsilon_k - q_k) - \gamma_k \pi_k$$

$$p_k = (\gamma_k - 1)c_{vk}T_k - \pi_k$$

$$\varepsilon_k = c_{vk}T_k + \frac{\pi_k}{\rho_k} \text{ Eq. 36}$$

The Stiffened Gas law is used for both gas and liquid. Parameters are summarized below:

$$\gamma_k = 1.4, \qquad c_{vk} = 1000, \qquad \pi_k = 0$$

$$\gamma_k = 4.4, \qquad c_{vk} = 4000, \qquad \pi_k = 6.10^8 \text{ Eq. 37}$$

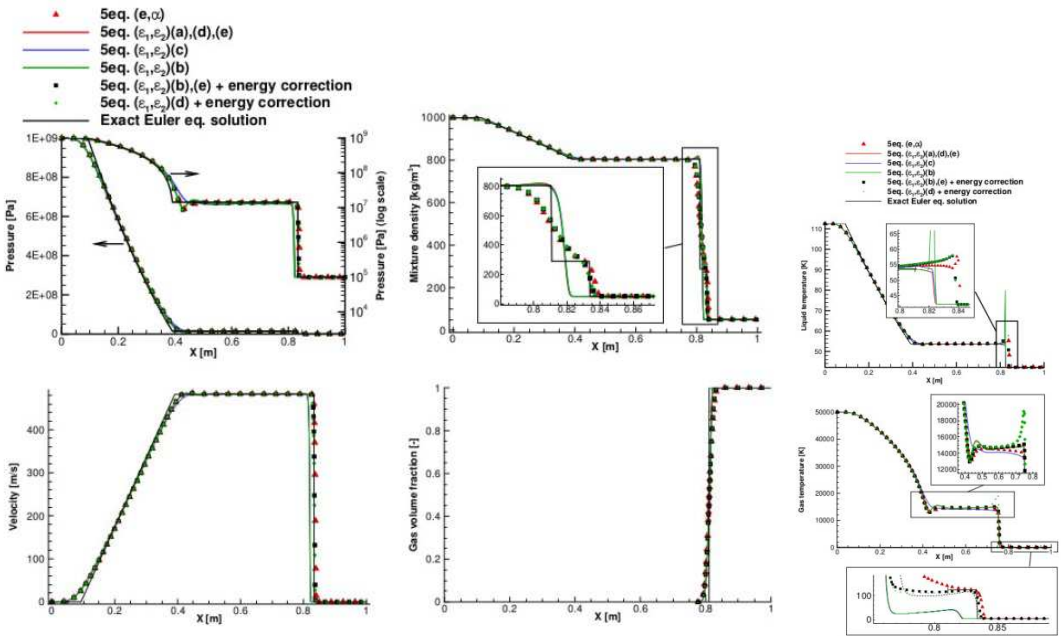

Figure 3: results of the 5 equation model with different HLLC schemes on the water air shock tube

3.2 Coaxial Injector LRE

In this last test case, we propose a three dimensional configuration of a coaxial cryogenic injector under subcritical conditions and based on the MASCOTTE [41] facility as depicted in figure 4. In order to reduce the mesh size and solution time, the simulation is performed with a 60° sector geometry. The geometry and the mesh are presented in figure 4. As seen in the Figure 4, the mesh is of course refined near the injection where the atomization takes place. Far from validation with experiments results, we want to show the enhancement of the coupling strategy with the 5 equation interface diffuse model. The law state for the LOx taking into account for liquid compressibility which has been used in the coaxial cryogenic injector test case reads:

$$\rho(T,p) = \frac{1}{v} = \frac{1}{v_0}\frac{1+\beta_0(P-P_0)}{1+\alpha_0(T-T_0)} \quad Eq.38$$

The different parameters for the oxygen are summarized below:

$P_0 = 10bar$
$T_0 = 85K$
$v_0 = 8{,}54.10^{-3} m^3/kg$
$\alpha_0 = 4.12\ 10^{-3}$
$\beta_0 = 1.71\ 10^{-9}$
$c_v = 951 J/kg/K$ Eq. 39

On the other hand a classical “perfect” Stiffened gas law state is used for the hydrogen GH_2:

$\gamma = 1.4$
$\pi = 0$
$c_v = 10112\ J/kg/K$ Eq. 40

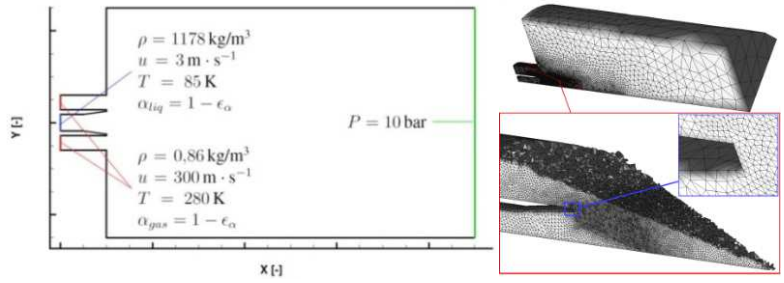

Figure 4: geometry and mesh of the coaxial injector

Figure 5: instantaneous visualization of the jet with droplets produced by atomization

Figure 6: iso-values of liquid volume fraction with atomization (upper side of the axis) and without atomization

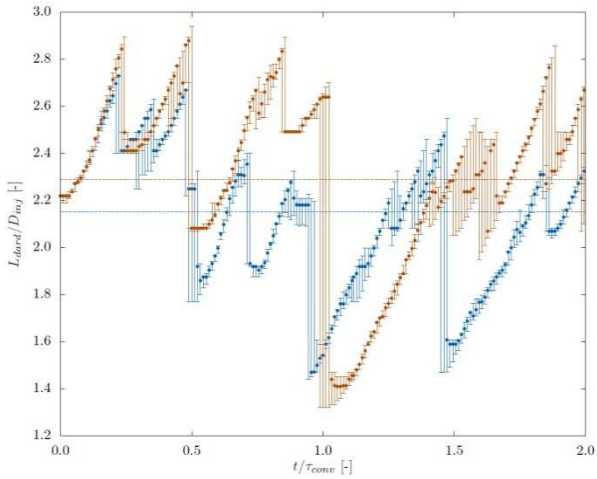

Figure 7: plot of liquid core length represented by volume liquid fraction between (α=0.95±0.04) over time with atomization (red) and without atomization (blue)

The capacity of the coupling strategy is illustrated in the following Figures. In Figure 5, we present an instantaneous visualization of the volume fraction of the liquid jet (iso-surface) as well as the particles generated by atomization. The physical time simulated corresponds to 74ms.

In Figure 6, we present two instantaneous iso-values field of the volume fraction at times 65ms and 74ms. This time interval corresponds to twice the convective characteristic convection time of the liquid core. We compare results obtained with atomization (upper side of the axis) and without atomization. (Color map legend: min = dark, max = white, with cutoff below = 0:01).

Moreover, quantitative result such as length of the liquid core is plotted. In the Figure 7, we present the liquid core representation thanks to iso-values of liquid volume fraction between [0.95±0.04]. The length of the liquid core renormalized by the injector diameter is plotted over time for two times the characteristic convection time (4,5ms) of the liquid core. We can observe instabilities along the axial direction. Comparison is made for the simulations with and without atomization. The length of the liquid core is also very similar when taking into account or not for atomization. This confirms that the atomization procedure has been carefully implemented. The results seem very promising.

4. CONCLUSION

We have successfully implemented a 5 equation interface diffuse model for the simulation of the dense “separated two-phase flow” within a coaxial LRE injector in sub-critical conditions. This new level of modelling allows us to perform accurate and robust simulations with a correct description of thermal transfer in the interface between liquid and gas. Moreover, the 5 equation model has been coupled with a spray kinetic solver following the fully Eulerian strategy proposed in our previous works. So, the atomization process has been taken into account and we have performed a difficult simulation showing very promising results. Concerning on going and future works, we intend to develop this Eulerian coupling strategy with a hierarchy of interface diffuse models and kinetic-based moment method (KBMM).

BIBLIOGRAPHY

[1] A. Andreini, C. Bianchini, S. Puggelli, F.X. Demoulin (2016). Development of a turbulent liquid flux model for Eulerian-Eulerian multiphase flow simulations. International Journal of Multiphase Flow. 81:88–103.

[2] P. A. Beau (2006). Modélisation de l’atomisation d’un jet liquide. Application aux sprays Diesel. Thèse de doctorat. Université de Rouen.

[3] A. Boucher (2016). Développement d'un modèle pour la simulation de l'atomisation dans les chambres de combustion des moteurs fusées à ergols liquides – Rapport d'activités 2016. RT 11/22894 DEFA.

[4] Z. Bouali, B. Duret, F.X. Demoulin, A. Mura (2016). DNS analysis of small scale turbulence scalar interaction in evaporating two phase flows. International Journal of Multiphase Flow. 85:326–335.

[5] M.R. Baer and J.W. Nunziato (1986). A two-phase mixture theory for the deflagration-to-detonation transition (DDT) in reactive granular materials. International Journal of Multiphase Flow. 12:861–889.

[6] J. Chesnel (2010). Simulation aux Grandes Échelles de l’Atomisation. Application à l’Injection Automobile. Thèse de doctorat. Université de Rouen.

[7] J. Chesnel, T. Menard, J. Reveillon, F.-X. Demoulin (2011). Subgrid analysis of liquid jet atomization. Atomization and Sprays. 21(1):41–67.

[8] J. Chesnel, J. Reveillon, T. Menard, F.-X. Demoulin (2011). Large eddy simulation of liquid jet atomization. Atomization and Sprays. 21(9):711–736.

[9] C. Crua, T. Shoba, M. Heikal, M. Gold, C. Higham (2010). High-speed microscopic imaging of the initial stage of diesel spray formation and primary breakup. SAE 2010–01–2247.

[10] F.X. Demoulin, P.A. Beau, G. Blokkeel, A. Mura, R. Borghi (2007). A new model for turbulent flows with large density fluctuations: application to liquid atomization. Atomization and Sprays. 17(4):315–345.

[11] B.M. Devassy, C. Habchi, E. Daniel (2015). Atomization modelling of liquid jets using a two-surface-density approach. Atomization and Sprays. 25(1):47–80.

[12] A. Desjardins, H. Pitsch (2010). Detailed numerical investigation of turbulent atomization of liquid jets. Atomization and Sprays. 20(4):311–336.

[13] F.-X. Demoulin, J. Reveillon, B. Duret, Z. Bouali, P. Desjonqueres, T. Menard (2013) Toward using direct numerical simulation to improve primary break-up modeling, Atomization and Sprays. 23 (11):957–980.

[14] B. Duret, J. Reveillon, T. Menard, F.X. Demoulin (2013). Improving primary atomization modeling through DNS of two-phase flows. International Journal of Multiphase Flow. 55:130–13.

[15] D. Fuster, A. Bague, T. Boeck, L. Le Moyne, A. Leboissetier, S. Popinet, P. Ray, R. Scardovelli, S. Zaleski (2009). Simulation of primary atomization with an octree adaptive mesh refinement and VOF method, International Journal of Multiphase Flow. (35)550–565.

[16] P. Gaillard, C. Le Touze, L. Matuszewski, A. Murrone (2016). Numerical Simulation of Cryogenic Injection in Rocket Engine Combustion Chambers, AerospaceLab Journal (11).

[17] P. Gicquel, E. Porcheron, E. Brisson (1998). Caractérisation expérimentale en combustion d'un brouillard LOX-GH2 issu d'un injecteur coaxial (campagne d'essais 1997 à 1 MPa). ONERA RT 98/6128 DEFA/Y/DMTE.

[18] M. Herrmann (2010). A parallel Eulerian interface tracking/Lagrangian point particle multi-scale coupling procedure. JCP. 229:745–759.

[19] M. Herrmann (2011). On simulating primary atomization using the refines level set grid method, Atomization and Sprays. 21(4):283–301.

[20] M. Ishii (2011). Thermo-fluid dynamics of two-phase flow. 2nd Edition, Springer, New York.

[21] S. Jay (2003). Modélisation de la combustion diphasique au moyen de bilans d'aire interfaciale et de surface de flamme. Application à la combustion cryotechnique. Thèse de doctorat. Ecole Centrale Paris.

[22] S. Jay, F Lacas, S Candel (2006). Combined surface density concepts for dense spray combustion. Combustion and Flame. 144(3):558–577.

[23] O. Le Métayer, J. Massoni, R. Saurel (2004). Elaborating equations of state of a liquid and its vapor for two-phase flow model. International Journal of Thermal Sciences. 43:265–276.

[24] S. LeMartelot, B. NKonga, R. Saurel. (2013). Liquid and liquid-gas flows at all speeds. JCP. 255:53–82.

[25] R. Lebas (2007). Modélisation Eulérienne de l'Atomisation Haute Pression - Influences sur la Vaporisation et la Combustion Induite. Thèse de doctorat. Université de Rouen.

[26] R. Lebas, T. Menard, P.A. Beau, A. Berlemont, F.X. Demoulin (2009). Numerical simulation of primary break-up and atomization: DNS and modelling study. International Journal of Multiphase Flow. 35:247–260.

[27] N. Meyers, (2006). Modélisation de la combustion cryotechnique avec prise en compte de l'atomisation primaire du jet d'oxygène liquide. Thèse de doctorat. Université d'Aix-Marseille II.

[28] C. Morel (2007). On the surface equations in two phase flows and reacting single phase flows. International Journal of Multiphase Flow. 33(10): 1045–1073.

[29] A. Murrone, N. Fdida, C. Le Touze, L. Vingert (2014). Atomization of cryogenic rocket engines coaxial injectors. Modeling aspects and experimental investigations. In: Space Propulsion. Cologne, Germany.

[30] A. Murrone and H. Guillard (2005). A five equation reduced model for compressible two-phase flow problems. JCP. 202:664–698.

[31] A. Murrone, C. Le Touze (2015). Eulerian coupling of two-phase flow models for the Large Eddy Simulation of the atomization in cryogenic combustion chamber. In 6th EUCASS.

[32] T. Menard, S. Tanguy, A. Berlemont (2007). Coupling level set/vof ghost fluid methods : validation and application to 3d simulation of the primary breakup of a liquid jet. International Journal of Multiphase Flows. 33(5):510–524.

[33] P. Marmottant, E. Villermaux (2004). On spray formation. Journal of Fluid Mechanics. 498:73–112.

[34] A. Murrone, P. Villedieu (2011). Numerical Modeling of Dispersed Two-Phase Flows. AerospaceLab Journal (2)

[35] A.R. Osta, J. Lee, K.A. Sallam, K. Fezzaa (2012). Study of the effects of the injector length/diameter ratio on the surface properties of turbulent liquid jets in still air using x-ray imaging. International Journal of Multiphase Flow. (38):87–98.

[36] M. Pourouchottamane (2002). Modélisation des brouillards denses pour la combustion cryotechnique. Thèse de doctorat. Université d'Aix-Marseille II.

[37] A. Refloch, B. Courbet, A. Murrone, P. Villedieu, C. Laurent, P. Gilbank, J. Troyes, L. Tessé, G. Chaineray, J. Dargaud, E. Quémerais, F. Vuillot (2011). CEDRE Software, AerospaceLab Journal (2).

[38] R. Saurel, R. Abgrall (1999). A Multiphase Godunov Method for Compressible Multifluid and Multiphase Flows. JCP. 150:427–460.

[39] R. Saurel, F. Petitpas and Ray A. Berry. (2009). Simple and efficient relaxation method for interfaces separating compressible fluids, cavitating flows and shocks in multiphase mixtures. Journal of Computational Physics. 228 (2009):1678–1712.

[40] A. Vallet (1997). Contribution à la Modélisation de l'Atomisation d'un Jet Liquide Haute Pression. Thèse de Doctorat. Université de Rouen.

[41] L. Vingert (2006). Sélection de cas tests Mascotte : - cas subcritique LOX/GH2 10 bar. - cas supercritique LOX/GH2 60 bar. Rapport technique RT 1/11785. ONERA.

[42] A. Vallet and R. Borghi (1999). Modélisation Eulerienne de l'atomisation d'un jet liquide, C.R. Acad. Sci. Paris Sér. II b, vol. 327(10):1015–1020.

[43] A. Vallet, A. Burluka and R. Borghi (2001). Development of an Eulerian model for the atomization of a liquid jet. Atomization and Sprays. 11:619–642.

[44] L. Vingert, M. Habiballah and J.C. Traineau (1999). MASCOTTE: a research facility for high pressure combustion of cryogenic propellants. In: 12th European Aerospace Conference.

[45] Wang, X. Liu, K.S. Im, W.K. Lee, J. Wang, K. Fezzaa, D.L.S. Hung and J.R. Winkelman (2008). Ultrafast x-ray study of dense liquid jet flow dynamics using structure tracking velocimetry, Nat. Phys., 4:305–309.

[46] A. Zein, M. Hantke, G. Warnecke. (2010). Modeling phase transition for compressible two-phase flows applied to metastable liquids. JCP. 229:2964–2998.